

Phase Diagram of Molecular Oxygen Adsorption on the (111) Platinum Surface

Xiao-Gang Wang^{1,2} and Galen B. Fisher^{1,*}

¹*Delphi Research Labs, Shelby Township, Michigan 48315, USA*

²*Department of Physics, Hunan Normal University, Hunan 410081, China*

(Received 20 February 2007; published 6 August 2007)

Molecular oxygen adsorption on the Pt(111) surface is studied based on *ab initio* computations and thermodynamics. An O₂ adsorption phase diagram is determined. There are two possible chemisorbed molecular states: one at a bridge site and another one at an fcc hollow site. While some population in the bridge sites persists at all coverages, the states coexist through the intermediate coverage phases. The relative coverage of the two species on the surface is determined by the competition between the Pt lattice distortion energy (that results from O₂ adsorption) and the O₂ repulsion energy. Our results give a reasonable explanation for the seemingly contradictory findings in previous experimental and theoretical work.

DOI: 10.1103/PhysRevLett.99.066101

PACS numbers: 68.43.Bc, 82.65.+r

A fundamental description of oxygen's adsorbed states on Pt surfaces is critical for understanding oxidation reactions on Pt, an important metal for many commercial applications, such as the oxidation of CO and NO_x in automotive exhaust and oxygen activation and hydrogen oxidation in fuel cells. Although considerable experimental and theoretical effort has been devoted to studying O₂ adsorption on the Pt(111) surface in the past few decades [1–12], our understanding is still limited. Even the adsorption configuration of molecular oxygen on the surface is a matter of controversy. The earliest electron energy loss spectroscopy (EELS) by Gland *et al.* [1] indicated a main vibrational band at 870 cm⁻¹ (see their Fig. 1) with a small band at 710 cm⁻¹. They assigned the 870 cm⁻¹ peak to the O-O stretching vibration of “lying-down” adsorbed O₂ on Pt(111). The experiments from Steininger *et al.* [2] found that at higher O₂ coverages, the O-O stretching vibration frequency of 875 cm⁻¹ is dominant, and with decreasing O₂ coverage, the concentration of an adsorbed state with an O-O frequency near 700 cm⁻¹ is increased. A very reported analogous results [3]. Scanning tunneling microscopy (STM) experiments [7] have also indicated two possible O₂ adsorbed states. However, near-edge x-ray-absorption fine-structure (NEXAFS) experiments [4] only observed one O₂ adsorbed oriented parallel to the Pt(111) surface, which was determined to have an O-O bond length of 1.37 ± 0.05 Å in later NEXAFS experiments [6] by some of the same authors. First-principles computations [8] showed that there are two possible O₂ adsorbed states on the Pt(111) surface: one adsorbed site is at the bridge site with an O-O stretching vibrational frequency of 850 cm⁻¹ and another one at the fcc site with the vibrational frequency of 690 cm⁻¹; the bridge site is energetically favored. The later STM experiment of Stipe *et al.* [9] identified the fcc site adsorption state. Using the same first-principles computation code as used in Ref. [8], Bocquet *et al.* [11] repeated the calculations and found that the fcc site adsorption is energetically favorable. The only difference between the two first-principles calculations is that

the earlier calculations are based on a rectangular $\sqrt{3} \times 2$ surface unit cell and the latter based on a hexagonal 2×2 unit cell, but the O₂ coverage for both of them is the same, 0.25 monolayer (ML). Here, we will report the first phase diagram for O₂ adsorbed on the Pt(111) surface, based on thermodynamics and first-principles computations. Our results give a reasonable explanation for the seemingly contradictory results from previous experimental and theoretical work.

For the ensuing computations, the Pt(111) (6 × 6) surface is employed, and the coverage increment of the O₂ molecular adsorption on the surface is 1/36 ML. The supercells include five Pt layers, and the O₂ molecules are adsorbed on one side of the slabs, and a 16 Å thick vacuum separates the slabs. A dipole correction was considered in our calculations [13]. For each O₂ coverage on the surface, no symmetry was forced in our supercells, and all possible configurations and adsorption sites within the supercell were considered. At equilibrium the total energy is minimized, and forces on all atoms are below 20 meV/Å. In our total-energy and force calculations, the exchange-correlation potential follows the generalized gradient approximation of Perdew [14] *et al.*, and the plane wave method [15] with the projector augmented wave method [16] is employed to solve the spin-polarized Kohn-Sham equations. The energy cutoff for the plane wave basis set is taken to be $E_{\text{cut}} = 320$ eV. A $2 \times 2 \times 1$ uniform **k**-point sampling is taken over the Brillouin zone.

What we desire is a phase diagram or knowledge of the adsorption phase configuration as a function of temperature and oxygen partial pressure. An accurate computation of the temperature and oxygen partial pressure dependence of this surface adsorption formation requires a thermodynamical method. The Gibbs free energy of adsorption ΔG for an surface adsorption phase x relative to the clean surface is given as follows:

$$\Delta G = G_x - G_{\text{clean}} - N_O \mu_O. \quad (1)$$

Here, G_x is the free energy for the adsorption phase x , and

G_{clean} is the free energy of the clean Pt(111) surface phase. N_{O} is the number of O atoms adsorbed on the surface (as dioxygen) in phase x , and μ_{O} is the chemical potential of O. $G_x - G_{\text{clean}}$ can be written as $G_x - G_{\text{clean}} = E_x^{\text{total}} - E_{\text{clean}}^{\text{total}} + P\Delta V + \Delta F_s(T)$. Here, E_x^{total} and $E_{\text{clean}}^{\text{total}}$ are the $T = 0$ K total energies of phase x and the clean phase, respectively. P is the pressure, ΔV is the volume difference between the two phases, and ΔF_s is the difference between the vibrational contributions of the two phases. It has been found [17,18] that the $P\Delta V$ term is very small compared with the total energy difference, $E_x^{\text{total}} - E_{\text{clean}}^{\text{total}}$. Since the mass of O is much smaller than that of Pt, we can approximately consider the effect of the local O vibration on the Pt vibration of the whole surface system to be small. ΔF_s mainly relies on the contribution of the O vibration and $\Delta F_s \approx \Delta F_s(N_{\text{O}}, T)$. The O vibration frequencies on the Pt(111) surface are obtained from our first-principles computation. Next, we take $\mu_{\text{O}} = \mu_{\text{O}}^0 + (KT \ln p)/2$, where μ_{O}^0 is the chemical potential of the standard state oxygen gas. Then, we take $\mu_{\text{O}}^0 = \mu_{\text{O}}^0(0) + \Delta\mu_{\text{O}}^0(T)$. The value of $\mu_{\text{O}}^0(0)$ is determined from our total energy calculations; $\Delta\mu_{\text{O}}^0(T)$ is an empirical value taken from the JANAF thermochemical tables [19]. Equation (1) can then be written as $\Delta G \approx \Delta G(T, p)$, and one can obtain the surface adsorption phase diagram as a function of the temperature, T , and oxygen partial pressure, p .

Experiments [1,3,20] have found that O_2 molecules at high coverages dissociate on the Pt(111) surface above 150 K. Here, we only want to investigate the adsorbed states of O_2 molecules in a thermodynamic environment. Hence, we limit the temperature to be below 150 K. Figure 1 shows the phase diagram of O_2 adsorption on the Pt(111) surface from 10–150 K and 10^{-30} to 1 atm. There are six possible adsorption phases, which depend on temperature and oxygen partial pressure. We found that

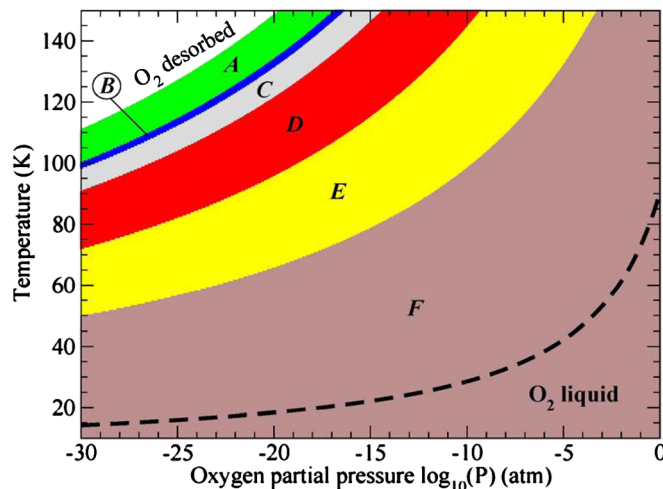


FIG. 1 (color online). Calculated phase diagram for O_2 adsorption on the Pt(111) surface for low temperatures and subatmospheric partial pressures of oxygen.

two chemical adsorbed states are energetically favorable over the whole temperature and pressure range. The first state is formed at the bridge site. The O_2 lies flat on the surface, and the two oxygen atoms are symmetrically located between the bridge sites with a bond length of 1.38 Å (0.028 ML O_2 coverage), as shown in Fig. 2. At the 0.028 ML O_2 coverage, the nearest distance of the oxygen atoms to Pt is 2.03 Å. An increase in the O_2 coverage changes the nearest distance and the O-O bond length less than ± 0.01 Å. The second state is formed at the fcc hollow site. One oxygen atom of the O_2 is located at a position slightly away from the center of the threefold fcc hollow towards the bridge site with a nearest distance of 2.18 Å to the Pt atoms. Another O atom is at a position near the atop site of the Pt atom with a nearest distance of 2.02 Å, also as shown in Fig. 2. This specie has its intramolecular axis at an angle of about 10.21° relative to the surface plane, similar to that found in Refs. [8,11]. The bond length of this O_2 is 1.41 Å. These values for the nearest distances and bond length are based on the 0.028 ML O_2 coverage. Increasing the coverage changes the value of the nearest distance to the Pt's for the O atom

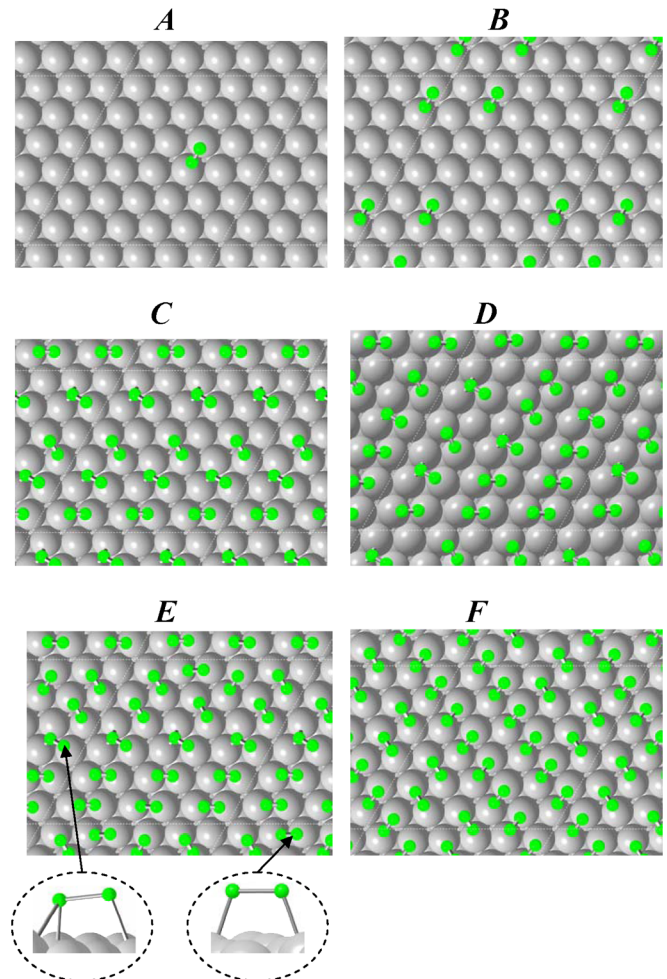


FIG. 2 (color online). The structures of the O_2 adsorption phases shown in Fig. 1 and Table I.

near the bridge site by $\sim -0.02 < \delta < 0.05$ Å, that to the Pt from the O atom near the atop site by less than ± 0.01 Å, and the O-O bond length by less than ± 0.02 Å. The two O₂ adsorbed states can exist in the same phase, but their coverage is different in the different phases, as shown in Table I.

At a higher temperatures and lower oxygen partial pressures, the 0.028 ML adsorbed phase **A** is energetically favorable, and O₂ occupies the bridge site. By either lowering the temperature or increasing the oxygen partial pressure, the phases transform in the order of **A** \rightarrow **B** \rightarrow **C** \rightarrow **D** \rightarrow **E** \rightarrow **F** and the O₂ coverage at the bridge sites increases with the phase transitions until the saturated coverage of 0.5 ML. However, the O₂ coverage at the fcc sites in phase **C** is 0.167 ML and then decreases to 0.083 ML in Phase **E**. The O₂ saturation coverage of 0.5 ML with all O₂ at bridge sites is consistent with experiment [2]. The dashed black line in the phase diagram indicates that below this line, the O₂ gas phase in the thermodynamic environment has changed to the O₂ liquid phase. The O₂ liquid may cover the surface and form an O₂ physically adsorbed state. This is consistent with the experiments [5,6] that found O₂ in a physically adsorbed state at very low temperatures.

It is interesting to see that the adsorption at bridge sites exists in all the possible phases, but the fcc sites adsorb O₂ just in Phases **C**, **D**, and **E**. Why does this happen? Our computations reveal that the surface distortion energy (defined as the total energy difference of the surface system with the structure distorted by the O₂ minus the total energy of the free surface system) plays a role as important as the repulsion energy between the O₂'s does. The adsorbed O₂ at the fcc hollow site creates a large distortion around the nearest threefold Pt atoms, which reduces by ~ 0.234 eV the energy increase of the surface system compared with the free Pt surface. The distortion energy reduced by the O₂ adsorption at the bridge site is ~ 0.152 eV, which is less than that reduced by adsorption at the fcc site. However, suitable mixed configurations of the fcc and bridge adsorptions of O₂ can give larger relative distances between the O₂'s, which can decrease the repulsion energy between the molecular species. Hence, the energetic competition between the changes in the distortion energy and the repulsion energy determines the popu-

lation of the possible O₂ adsorbed states: pure bridge adsorption, pure fcc hollow adsorption, or mixed fcc and bridge adsorption sites. The relative rate of coverage change between the fcc and bridge sites is decided by the competition also. We can see pure bridge site adsorption at lower coverages and then mixed adsorption in fcc and bridge sites as coverage increases, as shown in Table I. When the coverage is larger than 0.444 ML, the adsorbed state becomes pure bridge again since such a configuration can decrease the distortion energy, as shown in Fig. 2. The zero point vibrational energy also plays a role in the relative coverage of O₂ at the bridge and fcc sites. The value of the vibrational frequency of O₂ at the bridge site is 864 cm⁻¹ and that at the fcc site is 685 cm⁻¹, which makes a difference of ~ 0.02 eV/per O₂ between the two adsorption states.

We will now discuss why the relative adsorption energy between the bridge and fcc sites from Ref. [8,11] are different, although their calculations were based on the same computational code and the same O₂ coverage. Reference [8] shows that the adsorption energy at the bridge site is lower than that at the fcc site, but Ref. [11] shows the adsorption energy at the bridge site is higher than that at the fcc site. Our results reveal that this difference occurs because these references used different O₂ configurations at the surface although their O₂ coverage was the same, 0.25 ML. Reference [11] used a hexagonal 2×2 supercell configuration, while Ref. [8] used a rectangular $\sqrt{3} \times 2$ supercell configuration. The nearest distance between the O₂ molecules for the former is ~ 5.62 Å, and that for the latter is ~ 4.87 Å. We repeated their calculations, and our calculations were based on a 4×4 supercell in which O₂'s can be configured in either a 2×2 structure or a $\sqrt{3} \times 2$ structure. Our results indicate that for the 2×2 structure, the O₂ adsorption energy at the fcc site is a little lower (~ 0.003 eV/per O₂) than that at the bridge site, which is consistent with the result of Ref. [11], and for the $\sqrt{3} \times 2$ structure, the value of the O₂ adsorption energy at the fcc site is higher (0.081 eV/per O₂) than that at the bridge site, which is consistent with Ref. [8]. In the $\sqrt{3} \times 2$ configuration, the distortion energy reduced by O₂ at the fcc site is ~ 0.414 eV/per 4×4 supercell, but the reduction by O₂ at the bridge site is 0.378 eV. In the $\sqrt{3} \times 2$ structure, the nearest distance between the oxygen atoms of the O₂ molecules at the fcc sites is 3.485 Å and that at the bridge sites is 3.747 Å, which should make the repulsion energy between the dioxygen species at the fcc sites increase.

Now let us compare the experiments with our phase diagram. The EELS data of Gland *et al.* [1] show a main vibrational band at 870 cm⁻¹ and a small band at 710 cm⁻¹. They obtained the spectrum at 100 K and under $\sim 10^{-13}$ atm oxygen partial pressure. This thermodynamic environment falls into that of Phase **E** in which 0.361 ML O₂ occupies bridge sites and only 0.083 ML is at the fcc sites. Our calculations indicate that the 870 cm⁻¹ fre-

TABLE I. The coverage of chemisorbed O₂ at the fcc and bridge sites in the Pt(111) surface adsorbed phases.

Phases	fcc sites (ML)	Bridge sites (ML)	Total coverage (ML)
A	0.000	0.028	0.028
B	0.000	0.111	0.111
C	0.167	0.167	0.334
D	0.111	0.278	0.389
E	0.083	0.361	0.444
F	0.000	0.500	0.500

quency corresponds to the O-O stretching vibration at the bridge site, and other experiments [2,12] verified this also. The 710 cm^{-1} peak is very broad in the experimental spectrum in Fig. 1 of Ref. [1]. A similar peak is found at 700 cm^{-1} in Ref. [2], at 690 cm^{-1} in Ref. [3], and at 683 cm^{-1} in Ref. [12]. We believe these all correspond to the calculated O-O stretching vibration at the fcc site at 685 cm^{-1} in our calculation. In addition, the experiments from Steininger *et al.* and Avery [2,3] indicate that at higher O_2 coverage, the O-O stretching vibration with a frequency of 875 cm^{-1} is dominant, and with decreasing O_2 coverage, the 700 cm^{-1} O-O vibration is increased. This is consistent with our results. As shown in Fig. 1, when the O_2 coverage decreases, the phase changes according to the order, Phase $F \rightarrow E \rightarrow D \rightarrow C$ at 10^{-15} atm oxygen partial pressure (the experimental base pressure is $\sim 10^{-14}$ atm in [2]) and as shown in Table I, the bridge site coverage decreases, and the fcc site coverage increases from Phase F to C . Accessing Phases A and B and possibly Phase C is difficult to achieve experimentally because the lowest base pressures and partial pressures of oxygen measurable experimentally will be about $\sim 10^{-15}$ atm. Hence, we do not expect to find data with one bridging site at low coverages. At high coverages, we can see why NEXAFS experiments [4,6] found only one site, bridge site adsorption of O_2 . The O_2 adsorption states in the NEXAFS experiments of Outka *et al.* [4] were formed at 90 K and $\sim 10^{-11}$ atm oxygen partial pressure. The O_2 adsorbed phase under these conditions is Phase F in our phase diagram, in which only the bridge sites are occupied by O_2 's. The O_2 adsorption states in the NEXAFS experiments of Wurth *et al.* [6] were formed at 80 K, but they did not report the oxygen partial pressure. From our phase diagram, the adsorption phase is Phase F above 10^{-15} atm oxygen partial pressure at 80 K. Considering the pressure is $\sim 10^{-6}$ to 10^{-13} atm for a normal UHV system, the adsorption phase in the experiments of Wurth *et al.* [6] should be Phase F . Their experiments [6] also found that the adsorption is physical adsorption below 30 K. Our phase diagram shows that at 30 K and above $\sim 10^{-8}$ atm oxygen partial pressures, the O_2 gas phase is transformed into a liquidlike phase, and this O_2 state may cover the surface to form a physically adsorbed layer. This is supported by the physical adsorption seen experimentally at very low temperatures.

In summary, we present the first O_2 adsorption phase diagram for the Pt(111) surface, based on thermodynamics and first-principles computation. The phase diagram reveals that the O_2 adsorbed states on the Pt(111) surface are determined by their thermodynamic environment, the temperature, and oxygen partial pressure, and it predicts that (1) the bridge site adsorption state can exist alone both at higher temperatures and lower oxygen partial pressures and at high coverages at lower temperatures, and (2) that the bridge and fcc adsorption states can coexist through a range of coverages at intermediate temperatures and oxy-

gen partial pressures. The relative coverage of the two species is determined by the competition between the Pt lattice distortion energy produced by the adsorbed O_2 's and the repulsion between the O_2 molecules. Our results are quite consistent with available experiments and give a reasonable explanation for seemingly contradictory experimental and theoretical results, providing a framework for extending our understanding of the adsorption of molecules on metal surfaces.

We would like to deeply acknowledge and thank Dr. John R. Smith for his support and collaboration in much of this work. X.G.W. gratefully acknowledges the Project 10574041 supported by NSFC.

*Present address: Advanced Powertrain, Delphi Powertrain Systems, 51786 Shelby Parkway, Shelby Township, MI 48315-1786, USA

- [1] J. L. Gland, B. A. Sexton, and G. B. Fisher, *Surf. Sci.* **95**, 587 (1980); G. B. Fisher, B. A. Sexton, and J. L. Gland, *J. Vac. Sci. Technol.* **17**, 144 (1980).
- [2] H. Steininger, S. Lehwald, and H. Ibach, *Surf. Sci.* **123**, 1 (1982).
- [3] N. R. Avery, *Chem. Phys. Lett.* **96**, 371 (1983).
- [4] D. A. Outka, J. Stohr, W. Jark, P. Stevens, J. Solomon, and R. J. Madix, *Phys. Rev. B* **35**, 4119 (1987).
- [5] A. C. Luntz, J. Grimblot, and D. E. Fowler, *Phys. Rev. B* **39**, 12903 (1989).
- [6] W. Wurth, J. Stohr, P. Feulner, X. Pan, K. R. Bauchspiess, Y. Baba, E. Hudel, G. Rocker, and D. Menzel, *Phys. Rev. Lett.* **65**, 2426 (1990).
- [7] B. C. Stipe, M. A. Rezaei, W. Ho, S. Gao, M. Persson, and B. I. Lundqvist, *Phys. Rev. Lett.* **78**, 4410 (1997).
- [8] A. Eichler and J. Hafner, *Phys. Rev. Lett.* **79**, 4481 (1997).
- [9] B. C. Stipe, M. A. Rezaei, and W. Ho, *Science* **279**, 1907 (1998).
- [10] P. D. Nolan, B. R. Lutz, P. L. Tanaka, J. E. Davis, and C. B. Mullins, *Phys. Rev. Lett.* **81**, 3179 (1998).
- [11] M.-L. Bocquet, J. Cerda, and P. Sautet, *Phys. Rev. B* **59**, 15437 (1999).
- [12] (a) K. Gustafsson and S. Andersson, *J. Chem. Phys.* **120**, 7750 (2004); (b) *Phys. Rev. Lett.* **97**, 076101 (2006).
- [13] J. Neugebauer and M. Scheffler, *Phys. Rev. B* **46**, 16067 (1992).
- [14] J. P. Perdew, K. Burke, and M. Ernzerhof, *Phys. Rev. Lett.* **77**, 3865 (1996).
- [15] G. Kresse and J. Hafner, *Phys. Rev. B* **49**, 14251 (1994).
- [16] P. E. Blochl, *Phys. Rev. B* **50**, 17953 (1994).
- [17] C. G. Van de Walle and J. Neugebauer, *Phys. Rev. Lett.* **88**, 066103 (2002).
- [18] K. Reuter and M. Scheffler, *Phys. Rev. B* **65**, 035406 (2001).
- [19] D. R. Stull and H. Prophet, *JANAF Thermochemical Tables* (US. National Bureau of Standards, Washington, D.C., 1971), 2nd ed..
- [20] (a) J. Wintterlin, R. Schuster, and G. Ertl, *Phys. Rev. Lett.* **77**, 123 (1996); (b) T. Zambelli, J. V. Barth, J. Wintterlin, and G. Ertl, *Nature (London)* **390**, 495 (1997).